SLAC-PUB-1688
December 1975
(T/E)

DIMUON PRODUCTION BY NEUTRINOS: TEST OF WEAK CURRENT MODELS*

V. Barger
Stanford Linear Accelerator Center, Stanford University, Stanford, California 94305
and
Physics Department, University of Wisconsin, Madison, Wisconsin 53706

R. J. N. Phillips
Rutherford Laboratory, Chilton, Didcot, Oxon, England

T. Weiler
Physics Department, University of Wisconsin, Madison, Wisconsin 53706

ABSTRACT

We compare predictions of weak current models for $\mu^+\mu^-$ production initiated by ν and $\bar{\nu}$ with experimental x, y, p and v distributions of the muon associated with the incident neutrino. These distributions indicate that νN dimuon production occurs dominantly off valence quarks, with a y-dependence that is somewhat suggestive of $(1-y)^2$, while $\bar{\nu}N$ production occurs from sea quarks. Nevertheless, the original charm model provides a viable explanation within the uncertainties of present data. An improved description of the νN dimuon distributions is obtained with a V+A charm-changing current. The dimuon data do not exhibit the characteristics expected from the production of the b-type quark of vector-like theories. A vector meson dominance interpretation does not predict satisfactory x-dependences.

---

* Supported in part by the University of Wisconsin Research Committee with funds granted by the Wisconsin Alumni Research Foundation, and in part by the Energy Research and Development Administration Under contracts E(11-1)-881 and AT(04-3)515.

(Submitted to Phys. Rev.)

1. INTRODUCTION

The production and subsequent weak decay of hadrons with new quantum numbers is the most promising explanation of dimuon production by neutrinos and antineutrinos.[1,2] From the production characteristics of $\mu^+\mu^-$ events, it should therefore be possible to deduce information about the structure of weak current couplings to new quarks.

The original charm quark scheme,[3] which introduces one new quark c in addition to the (p, n, λ) triplet, leads to definite predictions for $\mu^+\mu^-$ distributions[4]— given our knowledge of deep inelastic scattering. The degree of success of these predictions can now be evaluated. Furthermore, recent theoretical speculations about the nature of the weak current have centered on a vector-like theory.[5,6,7,8] This involves the introduction of three generic-charm quarks (c, t, b) = (charm, top, bottom)[9] with charges (2/3, 2/3, -1/3) and V + A currents. If the new quarks have low enough masses to take part in weak production at present accelerator energies, then the dimuon data offer an excellent means to distinguish between competing theories.

Our purpose here is to compare observed $\mu^+\mu^-$ production characteristics with expectations from various charm current models, to see which models are favoured by experiment. We observe that the experimental x, y, and v distributions, of the muon associated with the incident neutrino, are best described by

(1) valence quark production by ν, with a y-dependence that is somewhat suggestive of $(1-y)^2$, and

(2) sea quark production by $\bar{\nu}$.

We find the 4-quark GIM charm model[3] provides a reasonable description of the dimuon data, within the present experimental uncertainties, but there are indications of possible disagreement with the νN data. In the GIM model, νN charm production comes from valence and sea partons in roughly equal proportions, with a constant y-dependence. A V + A charm-changing current[5,6,7,8,10,11] leads to better agreement with νN dimuon data, by enhancing the valence contribution, and by yielding a dominant $(1-y)^2$ dependence. However, the $\mu^+\mu^-$ distributions do not appear to have the production characteristics expected for the b-type quark of vectorlike weak current theories.[5,6,8]

Since each weak current model predicts a charm production rate, and the experimental dimuon rate is measured, a mean branching ratio

$$B = \Gamma(\text{charm} \rightarrow \mu + \text{anything})/\Gamma(\text{charm} \rightarrow \text{all})$$

for muonic decay of charmed hadrons is implied in each case. We assume that the mean muonic branching ratio does not differ strongly between the various charmed particles produced in different kinematic regions, and therefore does not bias the x- or y-distributions. For the GIM model a muonic branching ratio of order 10% is needed; with V + A currents a smaller value ≈ 5% is required.

2. KINEMATIC VARIABLES

The distributions of the "fast" μ^- (μ^+), associated with the incident ν ($\bar{\nu}$), can be compared directly with weak current models. The relevant variables are

$$v = \frac{2E'}{M} \sin^2 \frac{\theta'}{2} = xy \tag{1}$$

$$p = E(1-y) \tag{2}$$

$$y = \frac{E-E'}{E} = \frac{E'' + E_{\nu'} + E_H}{E} = \frac{\nu}{E} \tag{3}$$

$$x = v/y = Q^2/(2M\nu) \tag{4}$$

where the energies in the target nucleon rest frame are E (incident neutrino), E' (fast muon), E" (muon from decay), $E_{\nu'}$ (neutrino from decay) and E_H (final hadrons). The variables p and v are formally equivalent to x and y, but the x- and y-distributions are easier to interpret, being more simply related to the essential features of theoretical models.

In practice E is never well determined (even with narrow-band neutrino beams the resolution is poor and experimenters prefer to rely on the visible energy in the final state[2]). Since $E_{\nu'}$ is unobserved, x and y cannot strictly be measured in dimuon events. As alternatives, the variables

$$y_{VIS} = \frac{E_{VIS} - E'}{E_{VIS}} = \frac{E'' + E_H}{E' + E'' + E_H} \tag{5}$$

$$x_{VIS} = v/y_{VIS} \tag{6}$$

are used. They are bounded by

$$y_{VIS} \leq y \qquad , \qquad x_{VIS} \geq x \tag{7}$$

and reduce to y and x when

$$E_{\nu'}/(E'' + E_H) \ll 1 . \tag{8}$$

In practice we expect x_{VIS} and y_{VIS} distributions to approximate the true x and y distributions (see next section).

Experimental v and p distributions include all $\mu^+\mu^-$ events whereas x_{VIS} and y_{VIS} distributions can be formed only for calorimeter events for which E_H is measured. The total number of raw and corrected events in the HPWF distributions shown in the subsequent figures are

	v, p distributions		x, y distributions	
	raw events	corrected events	raw events	corrected events
ν	42	62	15	23
$\bar{\nu}$	16	24	8	13

3. EXPERIMENTAL CHARACTERISTICS OF DIMUON PRODUCTION

In the Harvard-Penn-Wisconsin-Fermilab (HPWF) experiment[1], dimuon events were observed in runs with widely different $\nu/\bar{\nu}$ flux ratios. The average properties of these dimuon events can be summarized as follows:

(i) νN cross sections for $E > 30$ GeV have the approximate ratios

$$\sigma_{\mu^-} : \sigma_{\mu^-\mu^+} : \sigma_{\mu^-\mu^-} = 1 : 10^{-2} : 10^{-3} \tag{9}$$

when averaged over the quadrupole triplet spectrum[1] (see Table 1 for details). No trimuon events were observed, even though detection efficiencies for trimuons and dimuons were comparable.

(ii) The signature of $\bar{\nu}$- induced $\mu^+\mu^-$ events is identified as $p^+ > p^-$ from a run with a dominant $\bar{\nu}$-flux. This allows a separation of ν and $\bar{\nu}$ initiated events.

(iii) The ratio of $\bar{\nu}$ to ν- induced $\mu^+\mu^-$ events is

$$\left(\sigma^{\bar{\nu}N}/\sigma^{\nu N}\right)_{\mu^+\mu^-} = 1.0 \pm 0.7 \tag{10}$$

based on

$$\left(\sigma^{\bar{\nu}N}/\sigma^{\nu N}\right)_{\mu} = 0.4 \ .$$

(iv) In ν - induced $\mu^{+}\mu^{-}$ events the average value of x^{-}_{VIS} is the same as the average value of x^{-} in single muon events.[12]

$$< x^{-}_{VIS} >_{\mu\mu} \simeq < x^{-} >_{\mu} \simeq 0.23 \ . \qquad (11)$$

For $\bar{\nu}$ - initiated events $< x^{+}_{VIS} >_{\mu\mu}$ is substantially smaller than $< x^{+} >_{\mu}$:

$$< x^{+}_{VIS} >_{\mu\mu} \simeq \frac{1}{4} < x^{+} >_{\mu} \simeq 0.06 \ . \qquad (12)$$

(v) For the $\mu^{+}\mu^{-}$ events the average energies are:

ν - initiated		$\bar{\nu}$ - initiated	
$< E' >$	$= 68 \pm 6$ GeV	$< E' >$	$= 41 \pm 6$ GeV
$< E'' >$	$= 11 \pm 1$	$< E'' >$	$= 13 \pm 2$
$< E_H >$	$= 39 \pm 7$	$< E_H >$	$= 37 \pm 7$
$< E_{VIS} >$	$= 114 \pm 14$	$< E_{VIS} >$	$= 85 \pm 10$

Based on an estimate $E_{\nu'} \sim E''$ for the decay leptons, we find that x and y would differ by only 10-20% from x_{VIS} and y_{VIS}. The y-distributions with $E_{\nu'} \sim E''$ are somewhat distorted towards large y-values, in comparison with the y_{VIS}-distributions. The x-distributions for $E_{\nu'} \sim E''$ are not significantly changed from the x_{VIS} distributions.

(vi) No dimuon events were observed for $0.8 \leq y_{VIS} \leq 1$ (see Fig. 1). The y-values calculated with the assumption $E_{\nu'} \sim E''$ also have $y \leq 0.8$ for all events. The deficiency at large - y could be due to poor experimental efficiency there or to a dynamical suppression, i.e. $d\sigma/dy \sim (1-y)^2$. In either case one also expects a depletion of events at small p, as seems to be the case (see Fig. 2).

(vii) From the experimental distributions of the minimum total mass W recoiling against the fast muon, the lower limits on the threshold for dimuon production are

$$\begin{aligned} W_{th} &\gtrsim 4\ \text{GeV} \quad \text{for } \nu \\ W_{th} &\gtrsim 5\ \text{GeV} \quad \text{for } \bar{\nu}\ . \end{aligned} \tag{13}$$

(viii) The seven observed $\mu^-\mu^-$ events show a different dependence on the azimuthal angle (in a plane normal to the neutrino beam) between the two muons from the $\mu^+\mu^-$ events, suggesting a different production mechanism. Five $\mu^+\mu^+$ events have also been observed.

The four fully measured νN dimuon events from the Caltech-Fermilab experiment[2] (CITF) have the following characteristics:

(i') All have opposite sign muons with $p^- > p^+$.

(ii') The value of $< x^-_{VIS} >$ for dimuon events is comparable to average x^- for single μ^- events.

(iii') The total observed energy $E_{VIS} = E' + E'' + E_H$ is close to the mean average energy of all ν_K-events, indicating that the unobserved final state neutrino carries only a small fraction of the available energy.

(iv') The $\mu^+\mu^-$ threshold could be as high as $W_{th} \simeq 10$ GeV, but this large value may be due to the experimental requirement that both muons penetrated the magnet.

The average properties of the CITF dimuon events are thus compatible with the higher-statistics HPWF results.

In our analysis, we shall make the approximate identification

$$x_{VIS} = x , \qquad y_{VIS} = y \tag{14}$$

suggested by experimental properties (v) and (iii'). Even with a more conservative approach in which the identification in Eq. (14) is not employed, we find that relative comparisons of the νN and $\bar{\nu} N$ x_{VIS} and y_{VIS} distributions provide valuable information on weak current models.

The HPWF and CITF results show clearly that $\nu N (\bar{\nu} N) \mu^+ \mu^-$ events generally obey the criterion $p_- > p_+$ $(p_+ > p_-)$. If a small fraction of events do not follow this criterion, they would be misassigned; however, after examining the data event by event, it appears that the slower muons are almost always below 20 GeV, and that misassigned events are unlikely to be biassing the x- or y-distributions dramatically.

The $\bar{\nu} N \mu^+ \mu^-$ events come from experimental runs involving three different incident flux spectra. We investigated the sensitivity of the calculations to the detailed $\bar{\nu}$ spectral mixing. The x-distribution calculations were insensitive to the mixing and the y-distribution calculations were only slightly changed by reasonable variations in the mixing.

4. QUARK PARTON MODEL FRAMEWORK

The x and y distributions of single muon events[12] are well described by the standard 3-quark parton model, for energies $E < 30$ GeV. The parton distributions have been determined[13] from the HPWF neutrino data, with a valence-sea separation

$$N_{VAL}(x) = p(x) + n(x) - \bar{p}(x) - \bar{n}(x) \tag{15}$$

$$N_{SEA}(x) = \bar{p}(x) + \bar{n}(x) = 2\lambda(x) = 2\bar{\lambda}(x) \; . \tag{16}$$

Here p(x), n(x), λ(x), etc. are the usual probability distributions for p, n, λ-type quarks in a proton target. The average x-values for the valence and sea components were found to be

$$< x_{VAL} > = 0.25 \tag{17}$$

$$< x_{SEA} > = 0.09 \; . \tag{18}$$

The single-muon data constrain the ratio of integrated sea and valence contributions

$$\epsilon = \frac{\int_0^1 x N_{SEA}(x)\,dx}{\int_0^1 x N_{VAL}(x)\,dx} \tag{19}$$

to lie in the range $0 \leq \epsilon \leq 0.12$, with the most reasonable choice being $\epsilon = 0.06$, which we shall use (solution 3 of Ref. 13).

A striking qualitative conclusion about the parton mechanism responsible for the dimuon events follows immediately from Eqs. (11)-(12) and Eqs. (17)-(18), namely

$$< x^{-}_{VIS} > \simeq < x_{VAL} > \tag{20}$$

$$< x^{+}_{VIS} > \simeq < x_{SEA} > \; . \tag{21}$$

Thus charm production by νN comes substantially from valence quarks, whereas charm production by $\bar{\nu}$N comes from the quark-antiquark sea. This property must be inherent in any acceptable charm-changing weak current model that explains the dimuon events. The existence of a quark-antiquark sea is thus directly indicated by the $\bar{\nu}$N dimuon data.

Taking parton distributions from single muon production (with symmetry arguments for the sea), the remaining degree of freedom is the charm production threshold. In view of the experimental uncertainty in W_{th} we consider two choices for the lowest charm threshold in our comparisons with data: $W_{th} = 4$ and 7.5 GeV.

Our evaluations of charm-changing weak current models are carried out within the framework of the quark parton model (QPM), with an SU(3) symmetric sea as in Eq. (16), neglecting charm-anticharm components of the nucleon sea. We treat the charm threshold by a θ-function in W, with immediate resumption of Bjorken scaling in x above threshold. Initially we focus our attention on $\mu^+\mu^-$ events, which are produced at a much higher rate than like-sign dimuons and which have the most direct theoretical interpretation.

5. GIM CHARM CURRENT

In the original charm quark model of Glashow, Iliopoulos and Maiani (GIM),[3] the weak currents arise from the left-handed doublets

$$\begin{pmatrix} p \\ n_C \end{pmatrix}_L \qquad \begin{pmatrix} c \\ \lambda_C \end{pmatrix}_L \tag{22}$$

where $n_C = nC + \lambda S$, $\lambda_C = \lambda C - nS$, $C = \cos\theta_C$, $S = \sin\theta_C$ and θ_C is the Cabibbo angle ($\sin^2\theta_C = 0.05$). The production of c via ν or $\bar{c}$ via $\bar{\nu}$, followed by weak decay with the emission of a muon, leads to $\mu^+\mu^-$ final states. In this model the charm production cross sections $\sigma(x,y) \equiv d^2\sigma/dxdy$ for an average nucleon target are

$$\sigma_c^{\nu N}(x,y)/x = N_{SEA}(x) + N_{VAL}(x)\, S^2 \tag{23}$$

$$\sigma_c^{\bar{\nu}N}(x,y)/x = N_{SEA}(x) \tag{24}$$

in units of $G^2 ME/\pi$.

All GIM $\bar{\nu}N\ \mu^+\mu^-$ production therefore comes from the sea; this agrees nicely with the x-distribution Eqs. (12) and (21). Taking $\epsilon = 0.06$, the $\nu N\ \mu^+\mu^-$ production comes about equally from valence and sea partons, giving $< x^-_{GIM} > = 0.16$ for $W_{th} = 4$ GeV; this is somewhat low but not really incompatible with Eq. (11), remembering the experimental uncertainties and the fact that $x \leq x_{VIS}$. The charm production ratio is then $\sigma_c^{\bar{\nu}N}/\sigma_c^{\nu N} \simeq \frac{1}{2}$, compatible with Eq. (10).

Spectrum averaged predictions of the GIM model are compared with the experimental $\mu^+\mu^-$ distributions in Figs. 1 and 2. We note the following points:

(i) The turnover of $d\sigma/dy$ at small-y is due to the kinematic constraint

$$y(1-x) \geq W_{th}^2/(2ME) \quad . \tag{25}$$

(ii) The agreement of the GIM model with the $\bar{\nu}N$ x- and v-distribution is excellent: the sharpness of the x^+_{VIS} data is correctly reproduced.

(iii) The broadness of the neutrino x^-_{VIS} distributions is adequately described by the model. The average values of x are

$$\begin{aligned} < x^-_{VIS} > &= 0.23 \pm 0.05 \\ < x^-_{GIM} > &= 0.16 \ . \end{aligned} \tag{26}$$

The valence contribution to Eq. (23) plays an important role. However the shape of the x^-_{VIS} distribution suggests that a higher proportion of valence contributions would be better.

(iv) The experimental $\bar{y}_{VIS}$ distribution tends to rise towards low y, while the predicted GIM y-distribution is flat.

(v) The effects noted above for x and y distributions are also reflected in p and v distributions (see Fig. 2).

(vi) For W_{th} = 4 GeV, the spectrum averages of the GIM cross sections for E > 30 GeV relevant to the experimental values in Eqs. (9) and (10), are

$$\begin{aligned} (\sigma_c/\sigma_\mu)^{\nu N} &= 0.08 \\ (\sigma_c/\sigma_\mu)^{\bar{\nu} N} &= 0.11 \\ \sigma_c^{\bar{\nu} n}/\sigma_c^{\nu N} &= 0.52 \end{aligned} \tag{27}$$

where $\sigma_\mu = \sigma(\text{non-charm}) + \sigma_c$. A mean muonic branching ratio of order

$$B \sim 0.1 \tag{28}$$

is required to agree with experiment Eq. (9). For a higher W_{th}, a higher value of B would be necessary. Muonic branching ratios as high as 20% are now considered to be theoretically acceptable.[14]

(vii) Overall, the GIM model is compatible[15] with the $\mu^+\mu^-$ data, but there are hints of disagreement with the νN x_{VIS} and y_{VIS} distributions.

The predictions of this and other weak-current models are summarized in Table 2. Their spectrum averaged cross sections are compared in Table 3.

6. VECTORLIKE THEORIES

In order to make the hadronic weak current vectorlike, six kinds of quarks are necessary. The weak current is then constructed from the following weak SU(2) doublets

$$\begin{pmatrix} p & c & t \\ n_C & \lambda_C & b \end{pmatrix}_L \qquad \begin{pmatrix} p & c & t \\ b & \lambda_{\tilde{C}} & n_{\tilde{C}} \end{pmatrix}_R . \tag{29}$$

Here the right-handed quarks are rotated by an angle

$$\begin{aligned} n_{\tilde{C}} &= n\cos\theta_{\tilde{C}} + \lambda\sin\theta_{\tilde{C}} \\ \lambda_{\tilde{C}} &= \lambda\cos\theta_{\tilde{C}} - n\sin\theta_{\tilde{C}} . \end{aligned} \tag{30}$$

Two versions of vectorlike models have been proposed, which we consider in turn. We shall consistently assume all "generic-charm" c, t, b components in the QPM sea to be negligible in our discussion.

I. De Rujula, Georgi, and Glashow (DDG)[5] take $\theta_{\tilde{C}} \simeq -\pi/2$ and assume charm thresholds W_c associated with c-quark production and $W_b = W_t > W_c$ associated with t and b-quark production.

For $W_c < W < W_t$ charm production involves only the weak current doublets[10]

$$\begin{pmatrix} c \\ \lambda_C \end{pmatrix}_L , \quad \begin{pmatrix} c \\ n \end{pmatrix}_R \tag{31}$$

The corresponding charm cross sections are[11]

$$\sigma_c^{\nu N}(x,y)/x = N_{SEA}(x)\left[1 + (1-y)^2\right] + N_{VAL}(x)\left[S^2 + (1-y)^2\right] \tag{32}$$

$$\sigma_c^{\overline{\nu} N}(x,y)/x = N_{SEA}(x)\left[1 + (1-y)^2\right]. \tag{33}$$

The most dramatic change from the GIM cross sections of Eqs. (23)-(24) is the greatly enhanced νN valence term with $(1-y)^2$ dependence; also the sea terms now have a y-dependence.

Spectrum averaged calculations of Eqs. (32) and (33) are compared with the experimental distributions in Figs. 3 and 4.

We make the following observations about the results:

(i) For $\bar{\nu}N$ the predictions are similar to the GIM case.

(ii) For νN the enhanced valence contribution gives better agreement with the x-dependence than the GIM model. Net valence and sea contributions to $\sigma_c^{\nu N}$ are now in the ratio five to one asymptotically, and for $W_c = 4$ GeV, we find

$$< x_{DGG}^- > \simeq 0.20 \quad . \tag{34}$$

(iii) The dominant new valence term in Eq. (32) has $(1-y)^2$ dependence, which gives better agreement with the y_{VIS}^- distribution.

(iv) The integrated contributions of $(1-y)^2$ terms are considerably smaller than 1/3, due to the threshold reduction at small y.

(v) For $W_c = 4$ GeV and $E > 30$ GeV, the spectrum averaged cross sections are

$$\begin{aligned} (\sigma_c/\sigma_\mu)^{\nu N} &= 0.23 \\ (\sigma_c/\sigma_\mu)^{\bar{\nu} N} &= 0.13 \\ \sigma_c^{\bar{\nu}N}/\sigma_c^{\nu N} &= 0.22 \quad . \end{aligned} \tag{35}$$

The predicted ratio of $\sigma_c^{\bar{\nu}N}/\sigma_c^{\nu N}$ is thus substantially reduced from the GIM prediction in Eq. (27) but still compatible with experiment Eq. (10). A mean muonic decay branching ratio $B \simeq 0.05$ is required, to agree with Eq. (9).

We conclude that the $\mu^+\mu^-$ x_{VIS} and y_{VIS} distributions are remarkably well described by the new charm current of Eq. (31). For this reason this model is an interesting candidate phenomenologically, despite theoretical difficulties with the $K_L - K_S$ mass difference and the PCAC analysis of $K \rightarrow 2\pi$ and $K \rightarrow 3\pi$ decays.[5, 8, 16, 17]

Thus far we have not considered charm contributions in the DGG model from the excitation of t and b quarks. For $W > W_2$ the currents associated with the doublets

$$\begin{pmatrix} p \\ b \end{pmatrix}_R \quad \begin{pmatrix} t \\ -\lambda \end{pmatrix}_R \tag{36}$$

produce the following <u>additional</u> charm cross section contributions

$$\sigma^{\nu N}_{b,t}(x,y)/x = N_{SEA}\left[1 + (1-y)^2\right] \tag{37}$$

$$\sigma^{\bar{\nu} N}_{b,t}(x,y)/x = N_{SEA}\left[1 + (1-y)^2\right] + N_{VAL}(x) \ . \tag{38}$$

The most significant addition is the valence contribution to $\bar{\nu}N$, which would lead to $< x^+_{VIS} > \simeq < x_{VAL} >$. Since this is not the case for the $\bar{\nu}N$ $\mu^+\mu^-$ events, there is no evidence yet for excitation of the b-quark. Since the W-distribution of $\bar{\nu}$ - induced $\mu^+\mu^-$ events extends up to 13 GeV, the b-quark must be substantially more massive than the c-quark to avoid conflict with this data. Predictions including b and t quark production at a higher common threshold, are shown in Fig. 5. Consistency of the model with the $\bar{\nu}N$ experimental x^+_{VIS} and v^+ distributions requires $W_b \gtrsim 10$ GeV.

II. Fritzsch, Gell-Mann, and Minkowski[6] (FGM) and Wilczek, Zee, Kingsley and Treiman[8] (WZKT) choose $\theta_{\tilde{C}} \simeq 0$. The charm changing weak currents are

$$\begin{pmatrix} t \\ n \end{pmatrix}_R \quad \begin{pmatrix} p \\ b \end{pmatrix}_R \quad \begin{pmatrix} c \\ \lambda_C \end{pmatrix}_L \quad \begin{pmatrix} c \\ \lambda \end{pmatrix}_R \ . \tag{39}$$

The charm cross-section components associated with the three thresholds W_t, W_b, and W_c are therefore

$$
\begin{aligned}
\sigma_t^{\nu N}(x,y)/x &= N_{SEA}(x)(1-y)^2 + N_{VAL}(x)(1-y)^2 \\
\sigma_b^{\nu N}(x,y)/x &= N_{SEA}(x) \\
\sigma_c^{\nu N}(x,y)/x &= N_{SEA}(x)\left[1+(1-y)^2\right] + N_{VAL}(x)\, s^2
\end{aligned}
\tag{40}
$$

$$
\begin{aligned}
\sigma_t^{\bar{\nu} N}(x,y)/x &= N_{SEA}(x)(1-y)^2 \\
\sigma_b^{\bar{\nu} N}(x,y)/x &= N_{SEA}(x) + N_{VAL}(x) \\
\sigma_c^{\bar{\nu} N}(x,y)/x &= N_{SEA}(x)\left[1+(1-y)^2\right] .
\end{aligned}
\tag{41}
$$

These expressions assume that the c, t, b components of the sea are negligible. If, as suggested, W_t is the lowest threshold and the thresholds W_b and W_c are substantially higher, the model has the following properties:

(i) $< x^- > \simeq < x_{VAL} >$ and $x^+ \simeq < x_{SEA} >$ as indicated experimentally.

(ii) Both $d\sigma/dy^-$ and $d\sigma/dy^+$ have a $(1-y)^2$ dependence.[8] This agrees well with the y^-_{VIS} data, and would explain the absence of dimuon events with $y^{\pm}_{VIS} > 0.8$. If the $\bar{t}t$ sea component were equal to that of the $\bar{p}p$ sea component, the y-dependence of $d\sigma/dy^+$ would be modified to $1 + (1-y)^2$.

(iii) For $W_{th} = 4$ GeV and $E > 30$ GeV, the spectrum averaged cross sections are

$$
\begin{aligned}
(\sigma_t/\sigma_\mu)^{\nu N} &= 0.18 \\
(\sigma_t/\sigma_\mu)^{\bar{\nu} N} &= 0.03 \\
\sigma_t^{\bar{\nu} N}/\sigma_t^{\nu N} &= 0.06 .
\end{aligned}
\tag{42}
$$

A mean muonic branching ratio of B ~ 0.05 is again required. The striking prediction of this model is the relative smallness of dimuon production by $\bar{\nu}N$ (~ 1/3 of GIM prediction) which, when coupled with the valence enhancement of νN production, gives a very small $\sigma_t^{\bar{\nu}N}/\sigma_t^{\nu N}$ ratio. However the $\bar{\nu}N$ dimuon production would be increased if the $\bar{t}t$ component of the sea were significant.

(iv) The W_b threshold must be high to avoid valence characteristics in the $\bar{\nu}N$ x^+_{VIS} and v^+ distributions.

The spectrum averaged charm production predictions, from the excitation of only the t-quark, are compared with the $\mu^+\mu^-$ distributions in Figs. 6 and 7. Predictions including c- and b-quark production as well, at a higher common threshold, are shown in Fig. 8. We note, for example, that with thresholds W_t = 4 GeV and $W_b = W_c \leq 10$ GeV, the model is not in accord with the $\bar{\nu}N$ experimental x^+ and v^+ distributions. We conclude that $W_b \gtrsim 10$ GeV.

Another possibility in the FGM-WZKT vectorlike model is to take W_c as the lowest threshold, with W_b and W_t much higher. In this case the predictions are rather similar to the GIM model. If we allow $\theta_{\tilde{C}}$ to be non-zero, there is an additional valence contribution in $\sigma_c^{\nu N}$ proportional to $(1-y)^2 \sin^2 \theta_{\tilde{C}}$, making the y-dependence less isotropic.

Still another possibility would be approximately degenerate W_t and W_c thresholds, with W_b much higher. In this case the FGM-WZKT predictions become similar to the c only results of the DGG model.

In summary, the vectorlike models of the weak current do not conflict with the dimuon data, provided that the masses of some of the quarks are sufficiently high to suppress their excitation in neutrino processes at present energies.

In fact the V + A current associated with an $n \rightarrow c$ or an $n \rightarrow t$ transition provides an excellent description of the $\nu N\, \mu^+\mu^-$ distributions. On the other hand the dimuon data provide no evidence in support of the proliferation of new quarks required in vectorlike theories. In particular the x and y distributions for $\bar{\nu} N\, \mu^+\mu^-$ events provides evidence that the b-quark is not being excited at present energies. If the b-quark exists in nature, its mass is likely to be so high that it is not relevant to e^+e^- physics at SPEAR energies. Consequently contributions from the b-quark should not be invoked in accounting for the magnitude that $R = \sigma(e^+e^- \rightarrow \text{hadrons})/\sigma(e^+e^- \rightarrow \mu^+\mu^-)$ has reached.

7. THRESHOLD CONSTRAINT FROM SERPUKHOV DIMUON SEARCH

From a search for dimuon production by neutrinos at Serpukhov[18], an upper bound of $\sigma_{\mu\mu}/\sigma_{\mu} \sim 10^{-3} - 10^{-4}$ was obtained for the energy range 6-30 GeV. Given a particular model prediction for σ_c, the Serpukhov bounds on $\sigma_{\mu\mu} = B\,\sigma_c$ can be transcribed into an upper limit on the branching ratio B. Using the calculated Serpukhov ν spectrum and an energy cut $E > 10$ GeV, the predictions in Table 4 for $(\sigma_c/\sigma_\mu)^{\nu N}$ were obtained. For consistency of the corresponding upper limits on B with our previous branching ratio estimates of $B \sim 0.1$ (GIM) and $B \sim 0.05$ (DGG or FGM-WZKT), a charm threshold of $W_c > 5$ GeV (GIM, DGG) or $W_t > 4$ GeV (FGM-WZKT) is indicated. It should be noted that these cross-section calculations for the threshold region of charm production are particularly dependent on our assumption that the charm contribution rescales in x. If a modified scaling variable were more appropriate[19], these near threshold cross section estimates would be reduced and the limits on B would be less restrictive (but B itself would increase somewhat). We conclude that the Serpukhov upper bounds on dimuon production are not inconsistent with a charm production threshold in the 4-5 GeV region.

8. DIMUON SUM RULES

The structure functions associated with single charm production can eventually be determined in narrow band experiments from high statistics $\mu^+\mu^-$ data. In the scaling region these structure functions should satisfy sum rules analogous to the Adler and Gross-Llewellyn-Smith sum rules for single muon structure functions. The dimuon sum rules are

$$\int_0^1 \left[F_1(x)^{\bar{\nu}N}_{\mu^+\mu^-} - F_1(x)^{\nu N}_{\mu^+\mu^-} \right] dx = (\Delta A)\, B \tag{43}$$

$$\int_0^1 \left[F_3(x)^{\bar{\nu}N}_{\mu^+\mu^-} + F_3(x)^{\nu N}_{\mu^+\mu^-} \right] dx = (\Delta B)\, B \tag{44}$$

where B denotes the mean branching ratio for muonic charm decay. The values of ΔA and ΔB associated with charm thresholds for various models are listed in Table 2. Similar sum rules can be written down for a hydrogen target. The sum rules hold even if c, t, b components exist in the sea.

9. LIKE-SIGN DIMUONS

The $\mu^-\mu^-$ events are produced by neutrinos at ~ 1/10 of the $\mu^-\mu^+$ rate. Like-sign dimuons, which do not come directly from the charm changing weak current, have several suggested origins:

(i) Associated production of charmed particles: If this is the explanation, trimuon events should eventually be observed at the level of $B\,\sigma_{\mu^-\mu^-}$. Moreover, about 4 of the 42 observed $\nu N\, \mu^+\mu^-$ events should likewise have an associated production origin. Assuming $B \leq 0.1$, associated charm production would have to take place at least at the 1% level.

(ii) D^o-$\overline{D}^o$ mixing: Transitions between neutral mesons of opposite charm, analogous to K^o-$\overline{K}^o$ mixing, would lead to final states with like-sign dimuons.[8,10] However a similar distribution in the azimuthal angle between the two muons would then be expected for $\mu^+\mu^-$ and $\mu^-\mu^-$ events, which does not seem to be the case.[1]

(iii) Several new quark types: weak production of a t-quark which then charge-exchanges into a b-quark before weak decay would lead to $\mu^-\mu^-$ events. However this mechanism requires a low threshold for b-quark production, which conflicts with observed characteristics of the $\overline{\nu}N\,\mu^+\mu^-$ distributions.

(iv) Existence of new quarks with charge $Q \geq 5/3$ or $Q \leq -4/3$.

10. VECTOR MESON DOMINANCE

In the vector meson dominance (VMD) approach,[20-27] charm production occurs through a coupling of the lepton current to charmed vector or axial vector mesons (D*, F*), which interact strongly with the nucleon target through their total cross sections. The dominant contribution in σ_{tot} at large W comes from the Pomeron exchange term. For F* mesons with $c\overline{\lambda}$ or $\lambda\overline{c}$ structure, there are no secondary Regge-pole exchanges and the Pomeron dominates even at small W. For charmed mesons with a p or n quark constituent, however, secondary Regge exchanges are allowed: the usual exoticity rules indicate that these will cancel out from σ_{tot} for $n\overline{c}$, $n\overline{t}$ and $p\overline{b}$ mesons, but will contribute positively in the crossed ($c\overline{n}$, $t\overline{n}$, $b\overline{p}$) channels. It is evident from duality diagrams that there is a one-to-one correspondence in quantum numbers and selection rules between the VMD Pomeron and the QPM sea, and between the VMD Regge and the QPM valence contributions. Qualitatively, at least, the VMD approach seems capable of duplicating most QPM results.

Quantitatively, however, it appears that VMD is not so successful. The charm production cross section for a pair of vector plus axial vector mesons of mass m has the general form

$$\sigma_c(x,y) = (\text{constant}) \frac{Q^2(1-x)}{(Q^2+m^2)^2} \left\{ \sigma_T\left[1+(1-y)^2\right] + 2\sigma_S(1-y) + \sigma_{int}\left[1-(1-y)^2\right] \right\} \tag{45}$$

with $Q^2 = 2MExy$. Here σ_T and σ_S are the sums of VN plus AN transverse and scalar total cross sections; σ_{int} is a V-A interference term related by the optical theorem to the imaginary part of the forward VN → AN amplitude. For the Pomeron, σ_T and σ_S are constants, and σ_{int} is expected to vanish; charm production is then the same for νN and $\bar{\nu}N$, at given ν, Q^2. Taking $m \simeq 2.2$ GeV, the resulting x-dependence is found to be similar to the valence distribution of QPM;[21] Figs. 9 and 10 illustrate the VMD Pomeron contributions (with $\sigma_S = 0$); the differences between νN and $\bar{\nu}N$ predictions stem from the differences of incident spectra.

The fact that the Pomeron x-distribution is broader than the corresponding QPM sea distribution makes the VMD approach much less satisfactory. For example, it is no longer possible to fit the $\bar{\nu}N$ x-distribution in any simple way. No doubt the model could be brought closer to the data by postulating a suitable (arbitrary) Q^2-dependence for σ_T, but it would then lose predictive power.

We do not pursue the y-dependence here, but it is interesting to note that the VMD Regge terms are by no means compelled to have the same y-dependence as QPM valence terms: it all depends on their spin-dependence and on the VN → AN amplitude (σ_T, σ_S and σ_{int}).

11. SINGLE MUON CROSS-SECTIONS

Although the charm production signal is more difficult to isolate experimentally in single muon production, such data nonetheless provide effective constraints on weak current models. In Fig. 11 we compare Fermilab total cross section data[28,29] for single μ production with predictions of GIM and vectorlike weak current models, taking the charm thresholds

$$\begin{array}{lll} \text{GIM} & \text{DGG} & \text{FGM-FZKT} \\ W_c = 4\ \text{GeV} & W_c = 4\ \text{GeV} & W_t = 4\ \text{GeV} \\ & W_b = W_t = 12\ \text{GeV} & W_b = W_c = 12\ \text{GeV}\ . \end{array} \tag{46}$$

The high effective threshold for b-excitations is necessary to avoid conflict with the $\bar{\nu}N$ dimuon data, in vectorlike models. The predictions for the energy dependence of average y of $\bar{\nu}N$ are shown in Fig. 12. We note that the FGM-WZKT model provides effectively no increase in $< y >^{\bar{\nu}N}$ below W_b, W_c thresholds. The predictions of the vectorlike models for $< y >^{\bar{\nu}N}$ below b-threshold will be larger if the $\bar{c}c$ and $\bar{t}t$ components of the sea are significant. The energy dependence of $< y >^{\bar{\nu}N}$ at small-x may thereby provide a sensitive measure of charm components of the sea.

12. CONCLUSIONS

The dimuon data provide a clean signal of the production of particles with new quantum numbers. Even with the present limited statistics the $\mu^+\mu^-$ events provide valuable information about the weak current production mechanism. Our principal conclusions regarding the $\mu^+\mu^-$ data can be summarized as follows:

(i) The x-distributions are well described by a quark sea for $\bar{\nu}N$ events, and a dominant quark valence contribution for νN events.

(ii) The GIM charm quark model[3] is compatible with the data but there are hints of disagreement in the νN x and y distributions that await experimental clarification. New V + A charm currents seem to provide a better description of the present data.

(iii) For W_{th} = 4 GeV the GIM scheme requires a mean muonic charm decay branching ratio $B \approx 0.1$ and predicts a $\bar{\nu}N/\nu N$ dimuon production cross section ratio near $\frac{1}{2}$. The DGG scheme with c-quark production requires a smaller value $B \simeq 0.05$ and predicts $\sigma_c^{\bar{\nu}N}/\sigma_c^{\nu N} \simeq 1/5$. The FGM-WZKT model with t-quark production also requires $B \approx 0.05$ and predicts $\sigma_t^{\bar{\nu}N}/\sigma_t^{\nu N} \simeq 1/16$. Raising W_{th} in any given model lowers the charm production cross section which implies increasing B.

(iv) Vectorlike theories[5,6,8] predict a valence contribution to the $\bar{\nu}N$ x-distribution above the threshold for production of the b-quark. The $\mu^+\mu^-$ data contain no evidence of such characteristics. Both the x-distributions and the $\bar{\nu}/\nu$ ratio exclude models[30] with a charmed quark of charge -4/3, that give valence-$\bar{\nu}$ and sea-ν charm production, with a large $\bar{\nu}/\nu$ ratio.

(v) If we exclude excitation of the b-quark, the apparently many choices of which quarks to excite in the above models reduce to just three groups (whose members are either identical or practically indistinguishable), namely

Group 1: GIM(c) $\simeq$ FGM-WZKT(c)

Group 2: DGG(c) $\simeq$ DGG(c + t) = FGM-WZKT(c + t)

Group 3: FGM(t)

where the symbols in brackets denote the quarks that are excited in the dimuon experiments. These are precisely the three QPM models we have illustrated.

(vi) Vector meson dominance models for charm production contain Pomeron and Regge exchange terms that obey the same selection rules as the sea and valence terms in a QPM description. However the VMD approach predicts too broad an x-dependence for the Pomeron term, and therefore does not fit dimuon data satisfactorily.

ACKNOWLEDGEMENTS

We are indebted to T. Y. Ling for providing detailed information about the HPWF dimuon data. We thank J. D. Bjorken, F. Gilman, G. Myatt, and G. Ringland for discussions.

REFERENCES

1. A. Benvenuti et al., Phys. Rev. Letters 34, 419 (1975); ibid 35, 1199 (1975); ibid 35, 1203 (1975); ibid 35, 1249 (1975).
2. B. C. Barish et al., Cal-Tech Report 58-485 (1975); B. C. Barish, Cal-Tech Report 68-510 (1975); A. Bodek, Cal-Tech Report 68-511 (1975).
3. S. L. Glashow, J. Iliopoulis, and L. Maiani, Phys. Rev. D2, 1285 (1970). Hereafter referenced as GIM.
4. V. Barger, T. Weiler and R. J. N. Phillips, "Charm Production by Partons in Neutrino Scattering," University of Wisconsin-Madison Report COO-441 (1975).
5. A. De Rujula, H. Georgi, and S. L. Glashow, "Vector Model of the Weak Interactions," Harvard preprint (1975). Hereafter referenced as DGG.
6. H. Fritzsch, M. Gell-Mann and P. Minkowski, "Vectorlike Weak Currents and New Elementary Particles," Cal-Tech Report 68-517 (1975). Hereafter referenced as FGM.
7. S. Pakvasa, W. A. Simmons, and S. F. Tuan, Phys. Rev. Letters 35, 702 (1975).
8. F. Wilczek, A. Zee, R. Kingsley and S. B. Treiman, "Weak Interaction Models with New Quarks and Right Handed Currents," FNAL PUB-75/44 THY. Hereafter referenced at WZKT. R. Kingsley, F. Wilczek, and A. Zee, Princeton preprint (1975).
9. H. Harari, SLAC-PUB-1568 (1975).
10. A. De Rujula, H. Georgi and S. L. Glashow, Phys. Rev. Letters 35, 69 (1975).

11. V. Barger, T. Weiler and R. J. N. Phillips, Phys. Rev. Letters 35, 692 (1975).

12. B. Aubert et al., Phys. Rev. Letters 33, 984 (1974); A. Benvenuti et al., Phys. Rev. Letters 34, 10, 597 (1875); D. Cline, rapporteur talk at Palermo Conference (1975).

13. V. Barger, T. Weiler and R. J. N. Phillips, "Parton Distributions from Neutrino Data," Nucl. Phys. (to be published).

14. J. Ellis, M. K. Gaillard, and D. V. Nanopoulos, CERN Report TH.2030 (1975); B. W. Lee, Fermilab Report Conference-75/72 -THY.

15. A. Pais and S. B. Treiman, "How Many Charm Quantum Numbers are There?," Princeton Report COO-223B-81 (1975). L. Wolfenstein, "Theory of Neutral Currents and Anomalous Neutrino Interactions," SLAC Conference (1975). B. W. Lee, "Dimuon Events," Fermilab-Conference-75/78-THY.

16. E. Golowich and B. R. Holstein, Phys. Rev. Letters 35, 831 (1975).

17. G. Branco, P. N. Mohapatra, and T. Hagiward, New York City College preprint (1975).

18. A. E. Asratyan et al., "Search for Muonic Pairs in the Neutrino Experiment at the IHEP 70 GeV Accelerator," IHEP Report 75-105.

19. A. De Rujula, H. Georgi, S. Glashow and H. Quinn, Rev. Mod. Phys. 46, 391 (1974). C. H. Llewellyn Smith, "Theory of Inelastic Lepton Interaction," SLAC Conference (1975).

20. B. A. Arbuzov, S. S. Gershtein and V. N. Folomeshkin, Phys. Letters 58B, 64 (1975).

21. V. Barger, T. Weiler and R. J. N. Phillips, "Vector Meson Dominance Calculations for the $\bar{\nu}$ Anomaly and Dimuon Production," Phys. Rev. (to be published); V. Barger, McGill Summer School Lectures (1975).

22. M. B. Einhorn and B. W. Lee, "Contributions of Vector-Meson-Dominance to Charmed Meson Production in Inelastic Neutrino and Antineutrino Interactions," Fermilab-Pub-75/56-THY (1975).

23. F. Hayot and H. T. Nieh, "Inelastic Neutrino Scattering: Nonscaling Effects at Large ω," SUNY Preprint ITP-SB-75-13.

24. J. Pumplin and W. Repko, Phys. Rev. D12, 1376 (1975).

25. M. K. Gaillard, S. A. Jackson and D. V. Nanopoulos, "Diffractive Elastic Neutrino-Production of Vector Mesons," CERN Report-TH-2049 (1975).

26. J. M. Wang and L. L. Wang, "Quark Description of Currents and Diffractive Contributions to Lepton Production," SUNY Report ITP-SB-75-28.

27. L. N. Chang, E. Derman and J. N. Ng, Phys. Rev. Letters 35, 1252 (1975).

28. D. Cline, rapporteur talk at Palermo Conference (1975). A. Mann, invited talk at Washington APS Meeting (1975).

29. B. C. Barish et al., Phys. Rev. Letters 35, 1316 (1975).

30. T. Goto and V. S. Mathur, Phys. Letters 59B, 153 (1975). F. E. Close and E. W. Colglazier, CERN Report TH.2065 (1975). K. V. L. Sarma and G. Rajasekran, Tata Preprint TIFR/TH/75-19. C. H. Albright and R. J. Oakes, Fermilab PUB 75-53-THY.

FIGURE CAPTIONS

Figure 1 Dimuon predictions of the GIM model for x and y distributions of the fast muons compared with HPWF data on x_{VIS} and y_{VIS}. N denotes corrected events per bin.

Figure 2 Dimuon predictions of the GIM model for v and p distributions of the fast muons compared with HPWF data.

Figure 3 Dimuon x and y predictions of the DGG vectorlike weak current model assuming c-quark production only at present energies.

Figure 4 Dimuon v and p predictions of the DGG vectorlike model assuming production of the c-quark only.

Figure 5 Dimuon x^+ and v^+ predictions of the DGG vectorlike weak current model for the c, b, and t quark production thresholds indicated.

Figure 6 Dimuon x and y predictions of the FGM-WZKT vectorlike weak current model, assuming production of the t-quark only at present energies.

Figure 7 Dimuon v and p predictions of the FGM-WZKT vectorlike model, assuming production of the t-quark only.

Figure 8 Dimuon x^+ and v^+ predictions of the FGM-WZKT vectorlike weak current model for the t, b, and c quark production thresholds indicated.

Figure 9 Dimuon x and y predictions from the vector meson dominance model of charm production, from Ref. 21.

Figure 10 Dimuon v and p predictions[21] from the vector meson dominance model.

Figure 11 Single muon total cross sections predictions from the GIM model and the vectorlike weak current models, with the thresholds of Eq. (46). The data are from Refs. 28 and 29.

Figure 12 Average y for single μ^+ events in $\bar{\nu}N$ as predicted by the GIM and vectorlike weak current models, with the thresholds of Eq. (46).

TABLE CAPTIONS

Table 1 Dimuon cross section and average x-values from the HPWF experiment.

Table 2 Predictions of weak current models for the νN and $\bar{\nu} N$ differential cross sections and for the QPM sum rules. The 3-quark contribution is common to all models. The charm contributions are separated according to c, t, b quark thresholds. The c, t, b components of the QPM sea are assumed to be negligible.

Table 3 Charm production cross sections from theoretical weak current models averaged over the quadrupole triplet spectrum for $E > 30$ GeV. To compare with the HPWF dimuon experimental results the σ_c/σ_μ ratios should be multiplied by the charm branching ratio into muons (B).

Table 4 Comparison of spectrum averaged predictions for $(\sigma_{\mu\mu}/\sigma_\mu)^{\nu N}$ with the upper limit of the Serpukhov experiment for $E > 10$ GeV.

TABLE 1

HPWF DIMUON DATA

$(\sigma_{\mu^+\mu^-}/\sigma_{\mu^-})^{\nu N}$	$(0.8 \pm 0.3) \times 10^{-2}$	Quadrupole Triplet Spe E > 30 GeV
$(\sigma_{\mu^+\mu^-}/\sigma_{\mu^+})^{\bar{\nu}N}$	$(2 \pm 1) \times 10^{-2}$	Combined Results 3 Sp E > 30 GeV
$(\sigma^{\bar{\nu}N}/\sigma^{\nu N})_{\mu^+\mu^-}$	$(0.8 \pm 0.6).(3\sigma^{\bar{\nu}N}_{\mu^+}/\sigma^{\nu N}_{\mu^-})$	E > 30 GeV
$(\sigma_{\mu^-\mu^-}/\sigma_{\mu^+\mu^-})^{\nu N}$	$(1.2 \pm 0.5) \times 10^{-2}$	Quadrupole Triplet Spe

Average x of Fast Muon in $\mu^+\mu^-$ and $\mu^\pm$ Events

	$< x_{VIS} >_{\mu\mu}$	$< x >_\mu$
νN	0.22 ± 0.04	0.23 ± 0.01
$\bar{\nu}N$	0.06 ± 0.02	0.23 ± 0.01

TABLE 2

MODEL	WEAK CURRENT DOUBLET	$\sigma(x,y)^{\nu N}/x$		$\sigma(x,y)^{\bar{\nu} N}/x$		SUM RULES	
		$N_{VAL}(x)$	$N_{SEA}(x)$	$N_{VAL}(x)$	$N_{SEA}(x)$	ΔA	ΔB
3-Quark	$\begin{pmatrix} p \\ n_C \end{pmatrix}_L$	C^2	$1 + (1-y)^2$	$(1-y)^2$	$1 + (1-y)^2$	$3S^2$	$-3(1+C^2)$
GIM							
c	$\begin{pmatrix} c \\ \lambda_C \end{pmatrix}_L$	S^2	1	0	1	$-3S^2$	$-3S^2$
VECTOR-LIKE (DGG)							
c	$\begin{pmatrix} c \\ \lambda_C \end{pmatrix}_L \begin{pmatrix} c \\ n \end{pmatrix}_R$	$S^2 + (1-y)^2$	$1 + (1-y)^2$	0	$1 + (1-y)^2$	$-3(1+S^2)$	$3(1-S^2)$
t	$\begin{pmatrix} t \\ -\lambda \end{pmatrix}_R$	0	$(1-y)^2$	0	$(1-y)^2$	0	0
b	$\begin{pmatrix} p \\ b \end{pmatrix}_R$	0	1	1	1	3	3
VECTOR-LIKE (FGM-WZKT)							
t	$\begin{pmatrix} t \\ n \end{pmatrix}_R$	$(1-y)^2$	$(1-y)^2$	0	$(1-y)^2$	-3	3
b	$\begin{pmatrix} p \\ b \end{pmatrix}_R$	0	1	1	1	3	3
c	$\begin{pmatrix} c \\ \lambda_C \end{pmatrix}_L \begin{pmatrix} c \\ \lambda \end{pmatrix}_R$	S^2	$1 + (1-y)^2$	0	$1 + (1-y)^2$	$-3S^2$	$-3S^2$

TABLE 3

MODEL	THRESHOLD	$(\sigma_c/\sigma_\mu)^{\nu N}$ (E > 30 GeV)	$(\sigma_c/\sigma_\mu)^{\bar{\nu} N}$ (E > 30 GeV)	$\sigma_c^{\bar{\nu} N}/\sigma_c^{\nu N}$ * (E > 30 GeV)
GIM	W_c = 4 GeV	0.08	0.11	0.52
	W_c = 7.5	0.05	0.06	0.47
VECTORLIKE (DGG)	W_c = 4	0.23	0.13	0.22
	W_c = 7.5	0.11	0.06	0.24
VECTORLIKE (FGM-WZKT)	W_t = 4	0.18	0.03	0.06
	W_t = 7.5	0.06	0.007	0.04

* Based on a reference value of $(\sigma^{\bar{\nu} N}/\sigma^{\nu N})_\mu = 0.4$ and to be compared with the HPWF value $(\sigma^{\bar{\nu} N}/\sigma^{\nu N})_{\mu\mu} = 1.0 \pm 0.7$.

TABLE 4

CONSTRAINTS IMPOSED BY SERPUKHOV DIMUON SEARCH

		$\sigma_{\mu\mu}/\sigma_{\mu}$ (E > 10 GeV)	Upper Limit on Muonic Branching Ratio B
SERPUKHOV EXPERIMENT		$\leq 0.52 \times 10^{-3}$	
GIM	$W_c = 4$ GeV	$37. \times 10^{-3} B$	$B \leq 0.02$
	$W_c = 5$	$13. \times 10^{-3} B$	≤ 0.04
	$W_c = 6$	$3. \times 10^{-3} B$	≤ 0.15
DGG	$W_c = 4$ GeV	$58. \times 10^{-3} B$	$B \leq 0.01$
	$W_c = 5$	$18. \times 10^{-3} B$	≤ 0.03
	$W_c = 6$	$3. \times 10^{-3} B$	≤ 0.15
FGM-WZKT	$W_t = 4$ GeV	$24. \times 10^{-3} B$	≤ 0.02
	$W_t = 5$	$4. \times 10^{-3} B$	≤ 0.12
	$W_t = 6$	$0.4 \times 10^{-3} B$	≤ 1.0

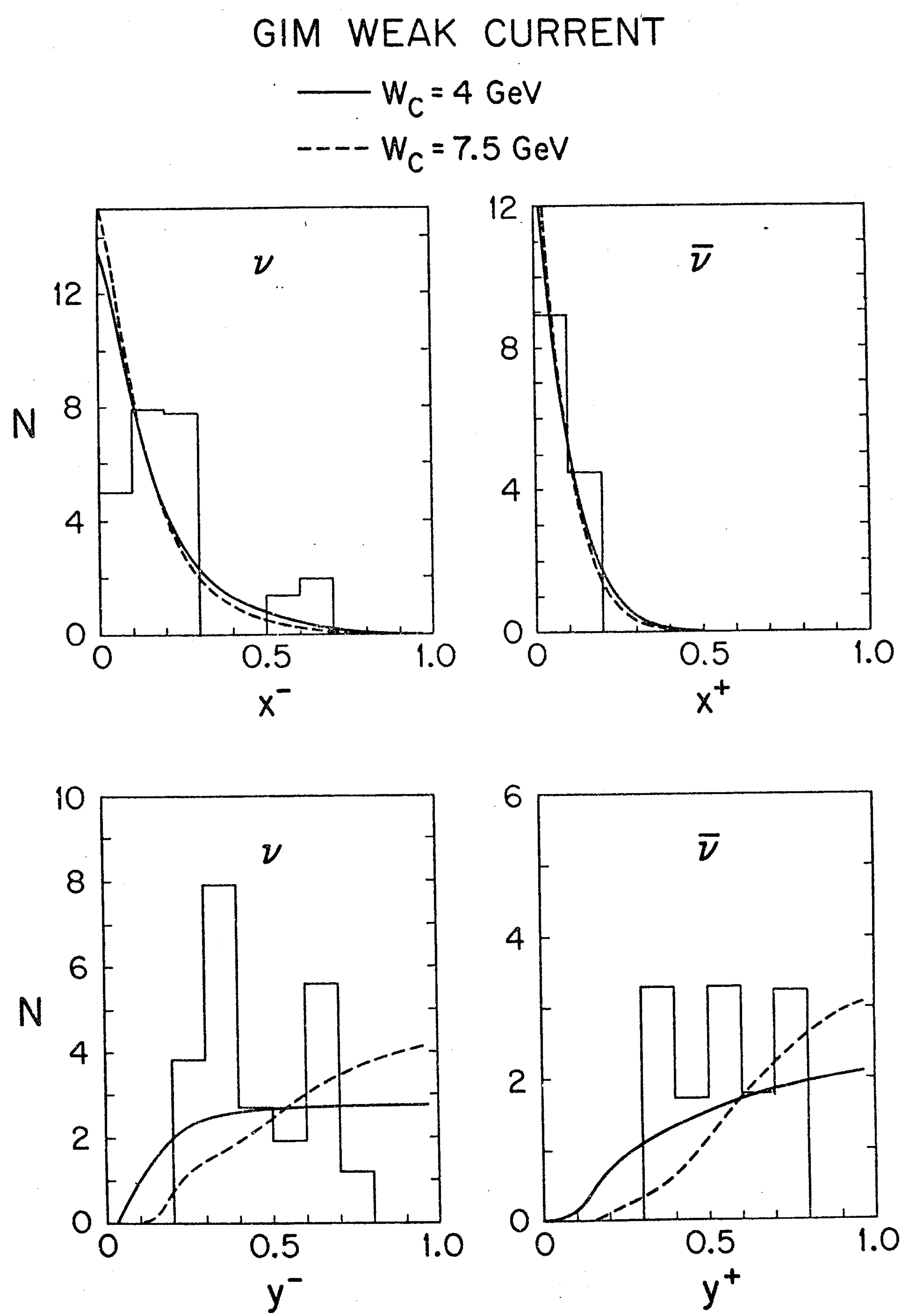

Fig. 1

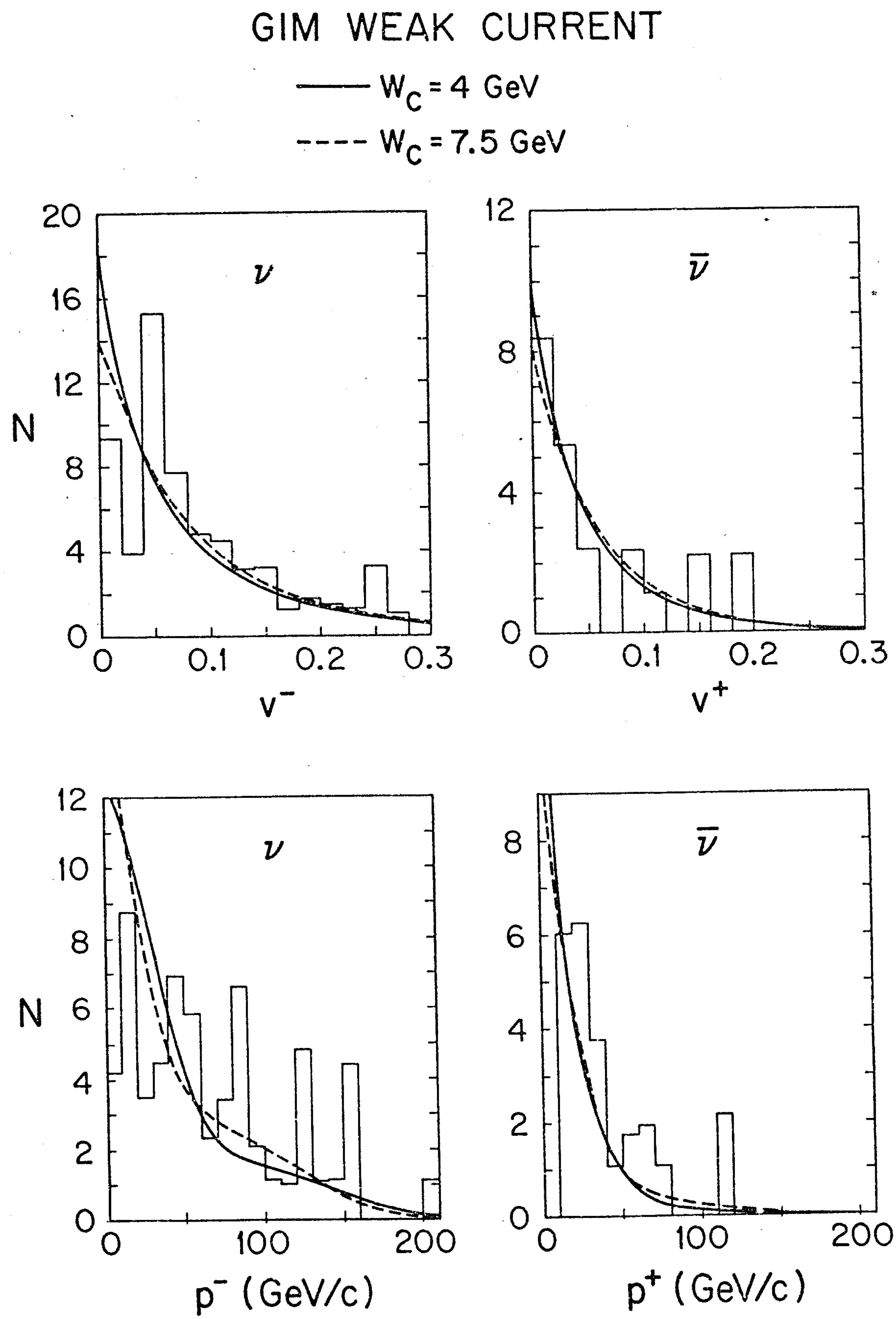
GIM WEAK CURRENT
$W_C = 4$ GeV
$W_C = 7.5$ GeV
N
ν
$\bar{\nu}$
20
16
12
8
4
0
0.1
0.2
0.3
v^-
v^+
10
6
2
100
200
p^- (GeV/c)
p^+ (GeV/c)

Fig. 2

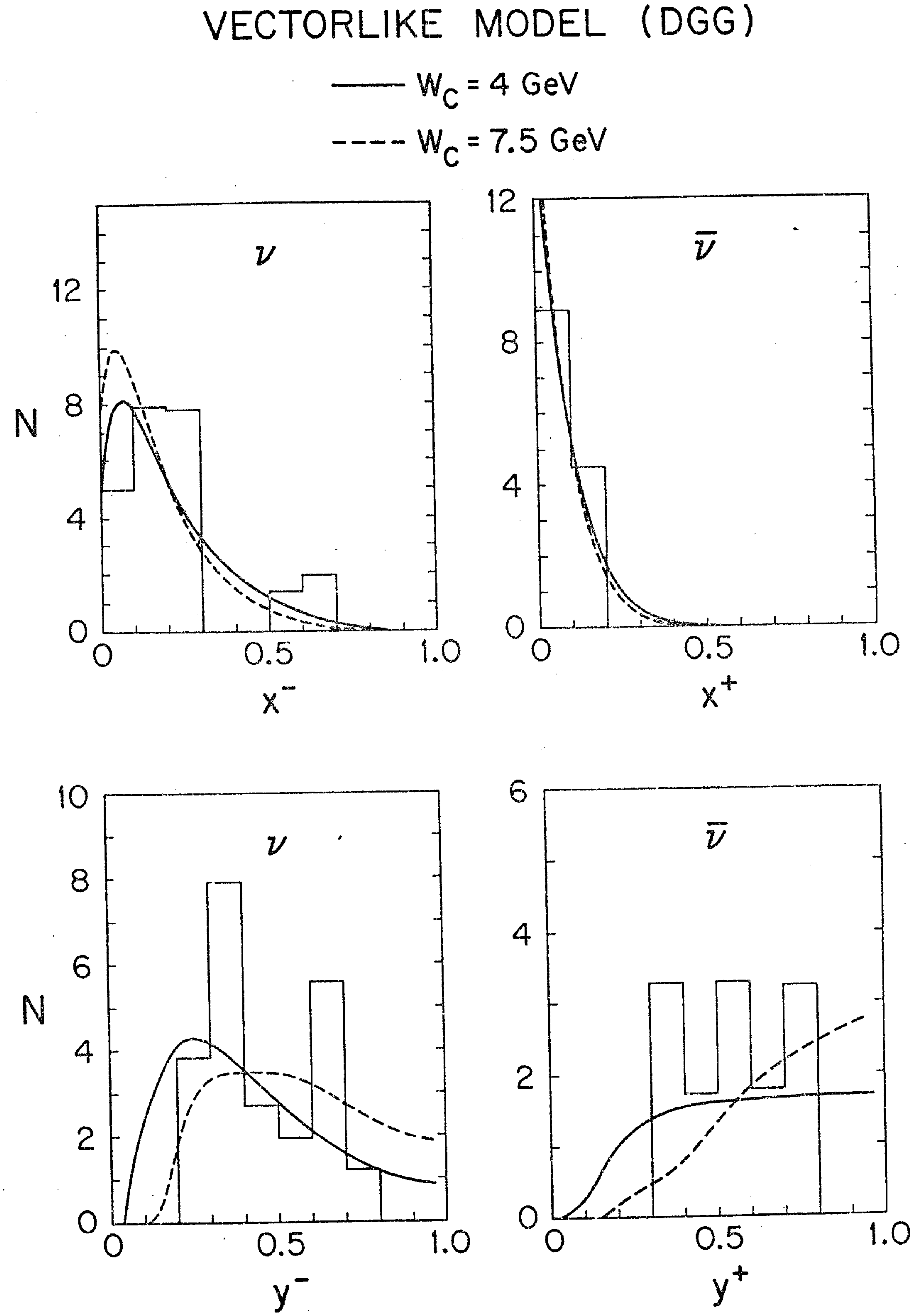

Fig. 3

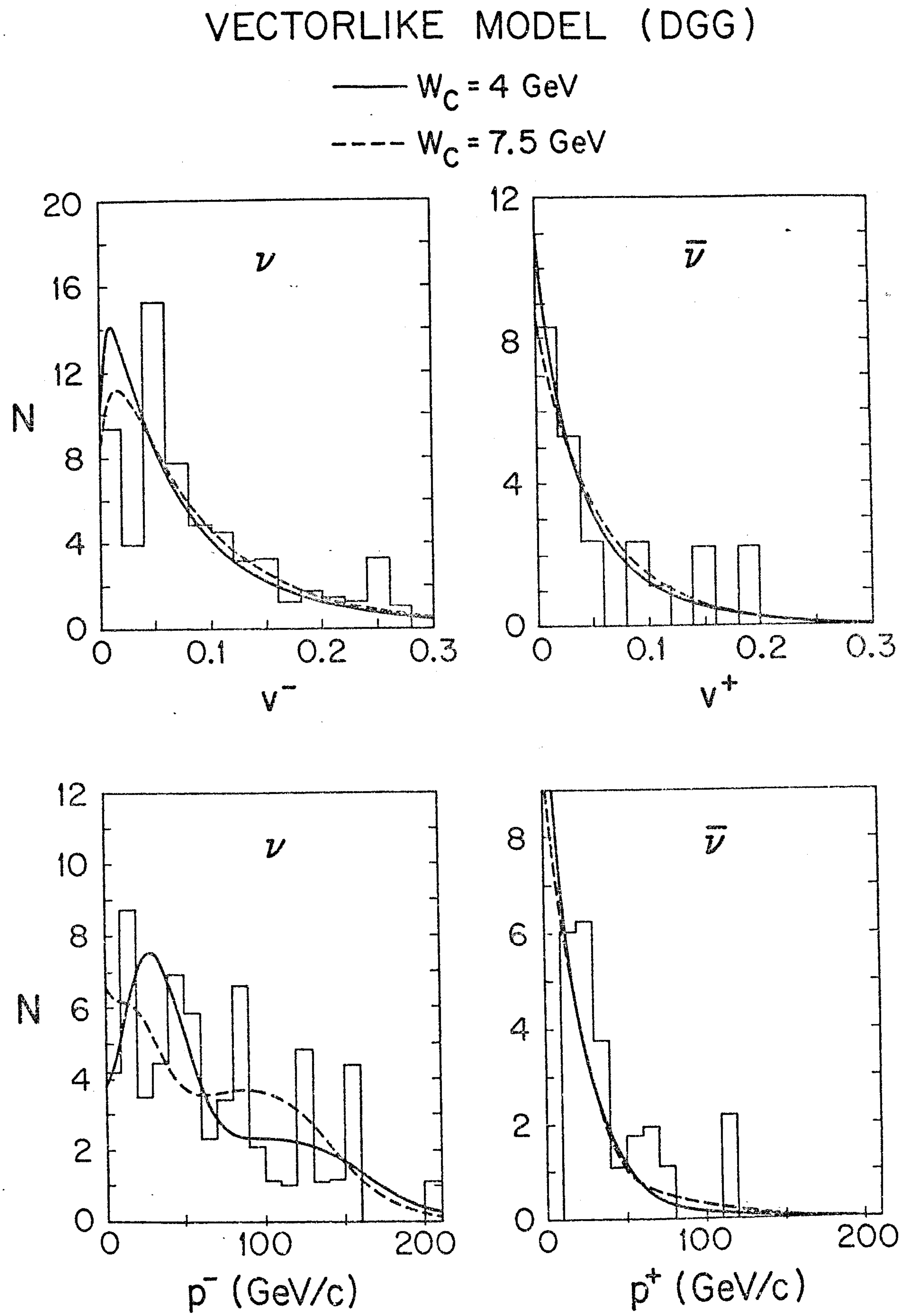
VECTORLIKE MODEL (DGG)
W_C = 4 GeV
W_C = 7.5 GeV
N
ν
$\bar{\nu}$
v^-
v^+
p^- (GeV/c)
p^+ (GeV/c)
0
4
8
12
16
20
0.1
0.2
0.3
2
6
10
100
200

Fig. 4

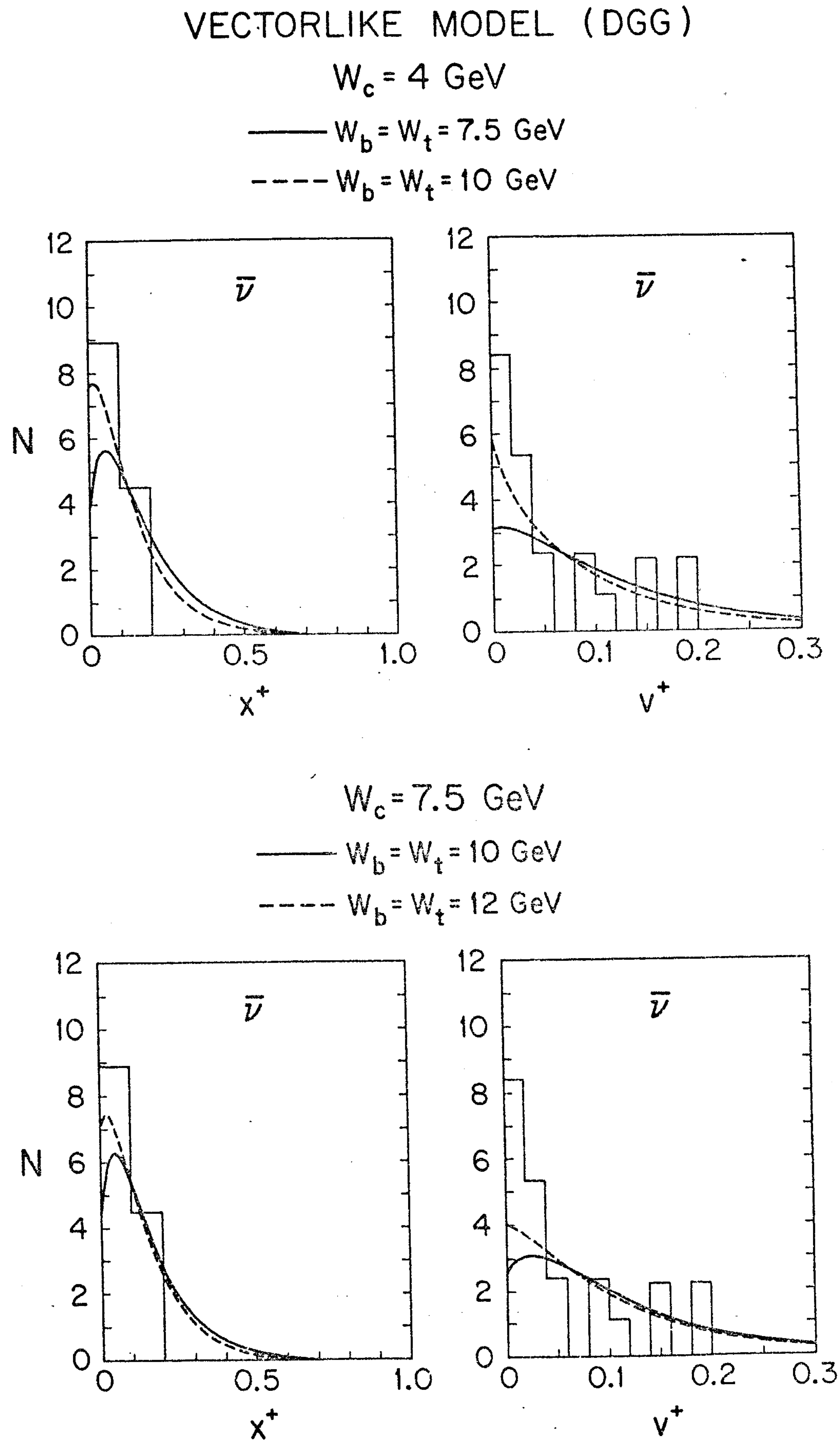
VECTORLIKE MODEL (DGG)
W_c = 4 GeV
$W_b = W_t$ = 7.5 GeV
$W_b = W_t$ = 10 GeV
W_c = 7.5 GeV
$W_b = W_t$ = 10 GeV
$W_b = W_t$ = 12 GeV
N
$\bar{\nu}$
x^+
v^+

Fig. 5

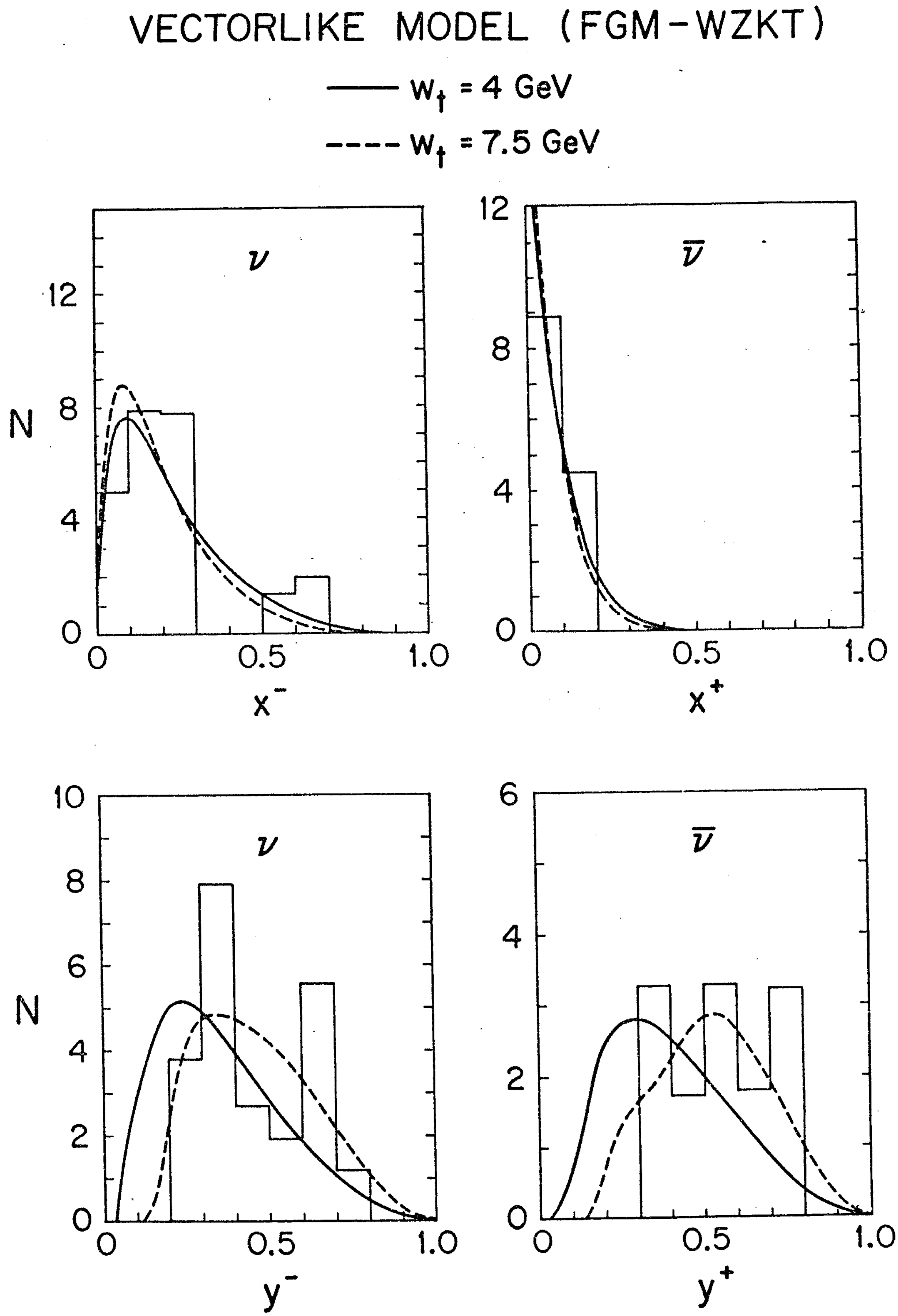
VECTORLIKE MODEL (FGM-WZKT)
W_t = 4 GeV
W_t = 7.5 GeV
ν
$\bar{\nu}$
N
x^-
x^+
y^-
y^+
0
0.5
1.0
4
8
12
2
6
10

Fig. 6

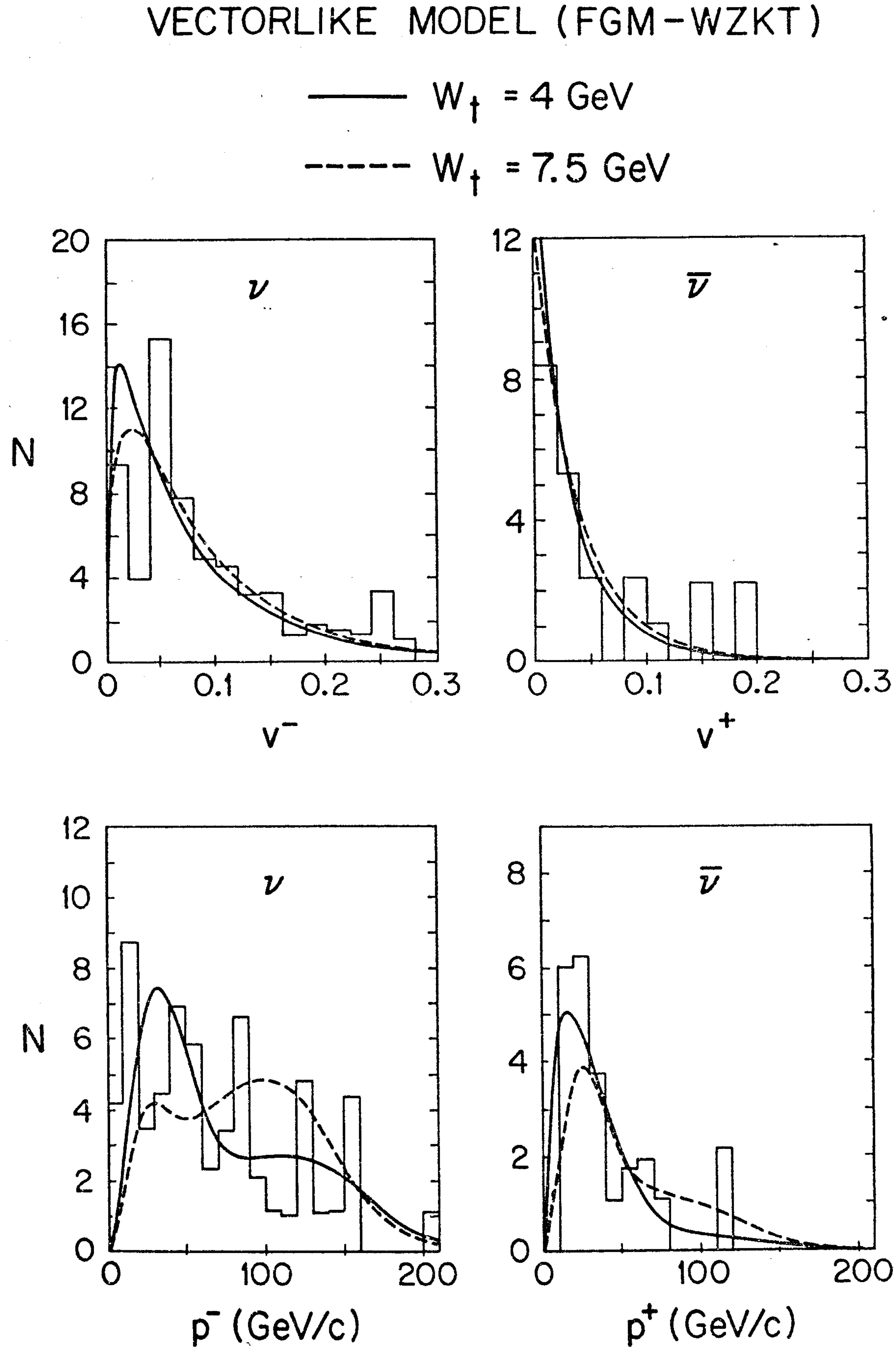
VECTORLIKE MODEL (FGM-WZKT)
W_t = 4 GeV
W_t = 7.5 GeV
ν
$\bar{\nu}$
N
v^-
v^+
p^- (GeV/c)
p^+ (GeV/c)
0
0.1
0.2
0.3
4
8
12
16
20
2
6
10
100
200

Fig. 7

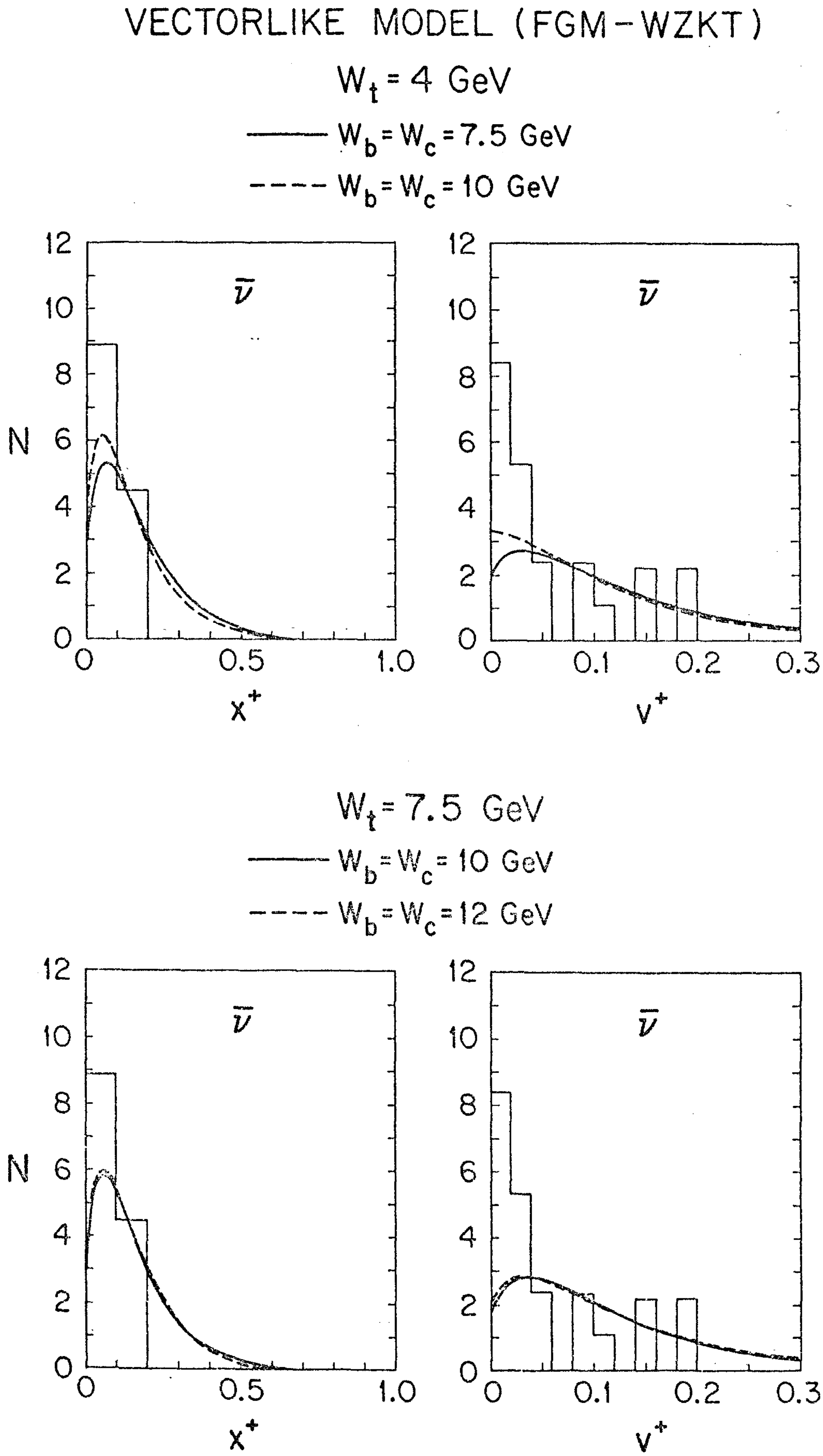
VECTORLIKE MODEL (FGM-WZKT)
$W_t = 4$ GeV
$W_b = W_c = 7.5$ GeV
$W_b = W_c = 10$ GeV
$\bar{\nu}$
$\bar{\nu}$
N
x^+
v^+
$W_t = 7.5$ GeV
$W_b = W_c = 10$ GeV
$W_b = W_c = 12$ GeV
$\bar{\nu}$
$\bar{\nu}$
N
x^+
v^+

Fig. 8

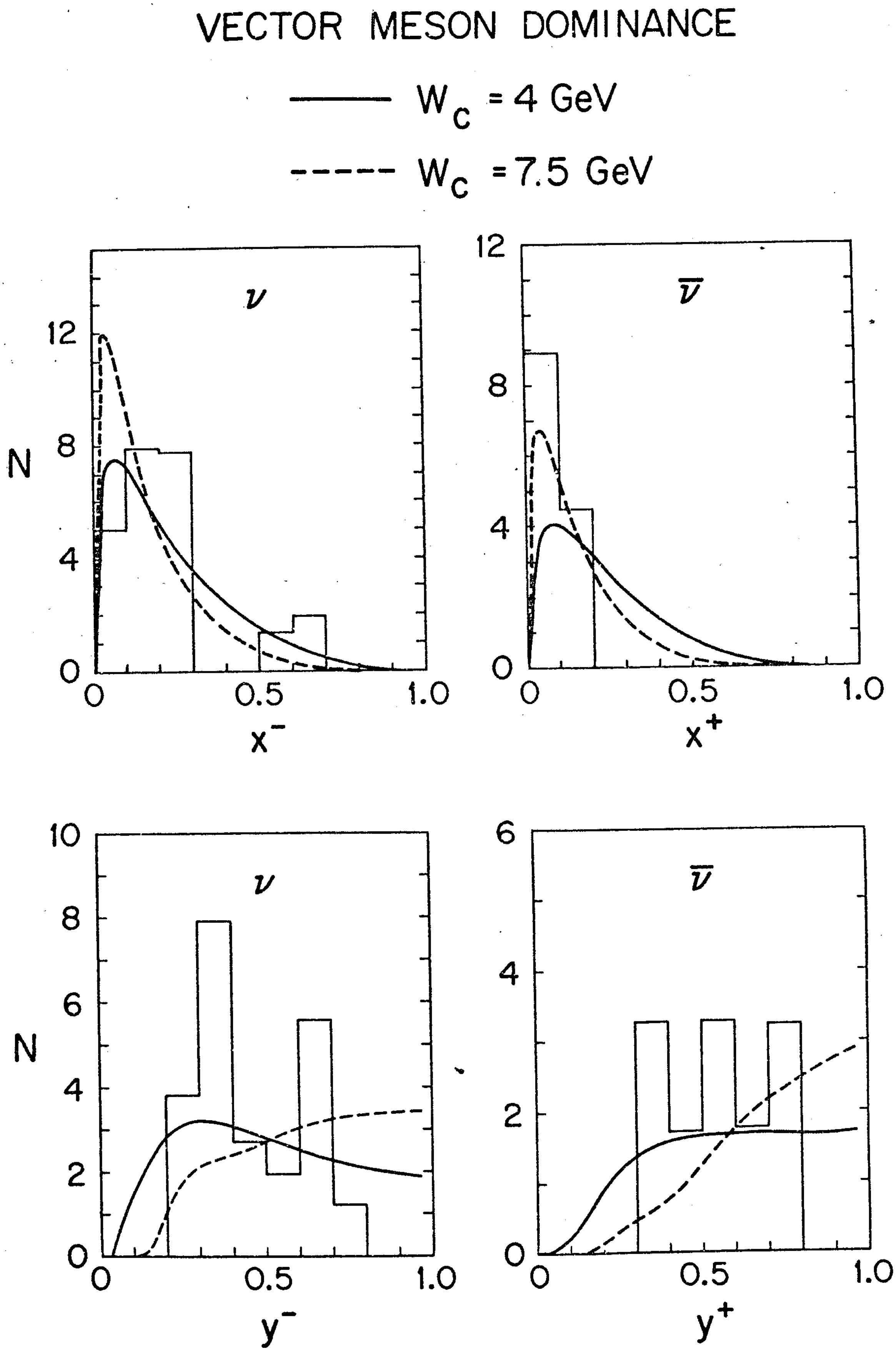
VECTOR MESON DOMINANCE
W_c = 4 GeV
W_c = 7.5 GeV
ν
ν̄
N
x⁻
x⁺
y⁻
y⁺
0
0.5
1.0
4
8
12
2
6
10

Fig. 9

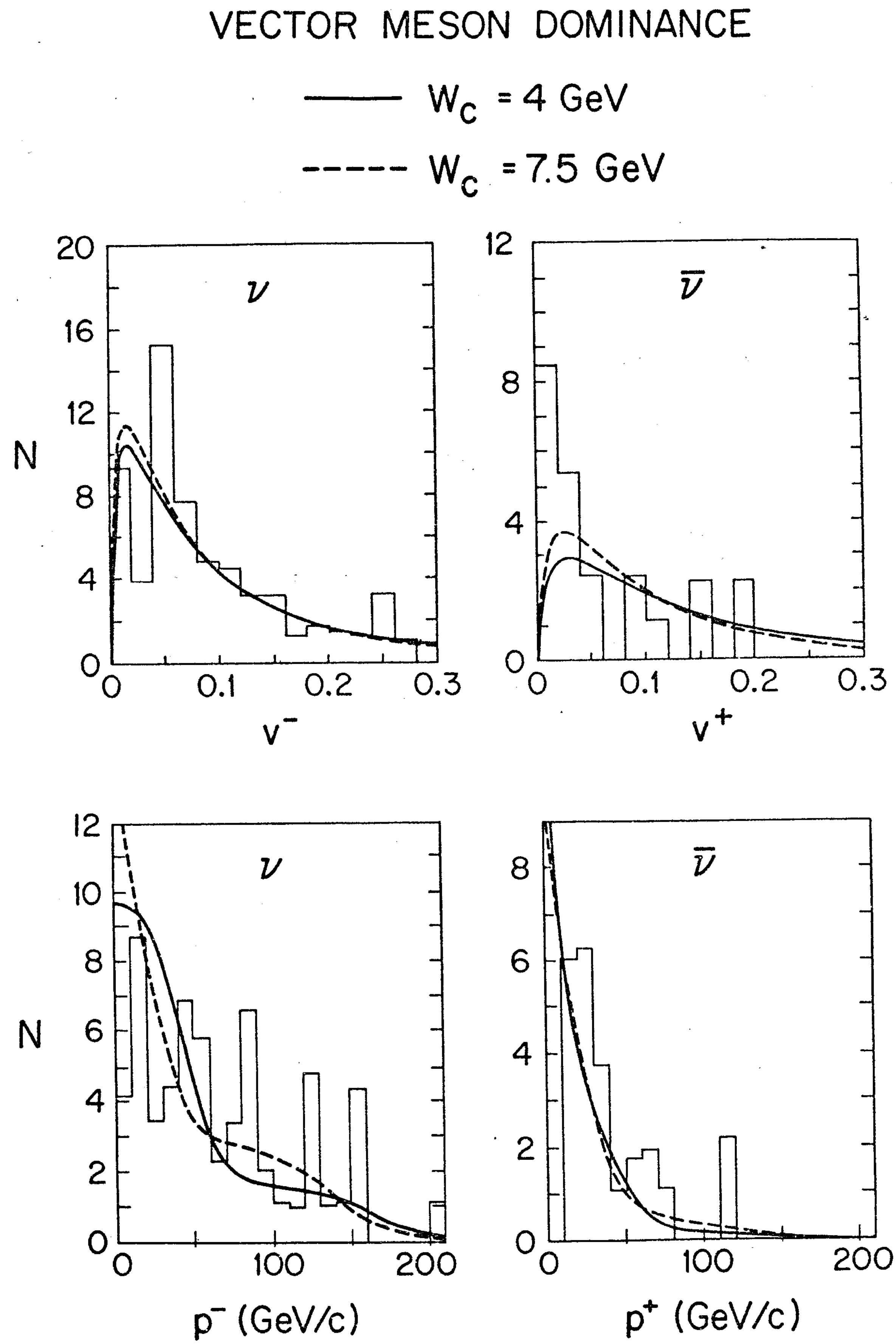
VECTOR MESON DOMINANCE
W_c = 4 GeV
W_c = 7.5 GeV
N
ν
$\bar{\nu}$
20
16
12
8
4
0
0.1
0.2
0.3
v^-
v^+
10
6
2
100
200
p^- (GeV/c)
p^+ (GeV/c)

Fig. 10

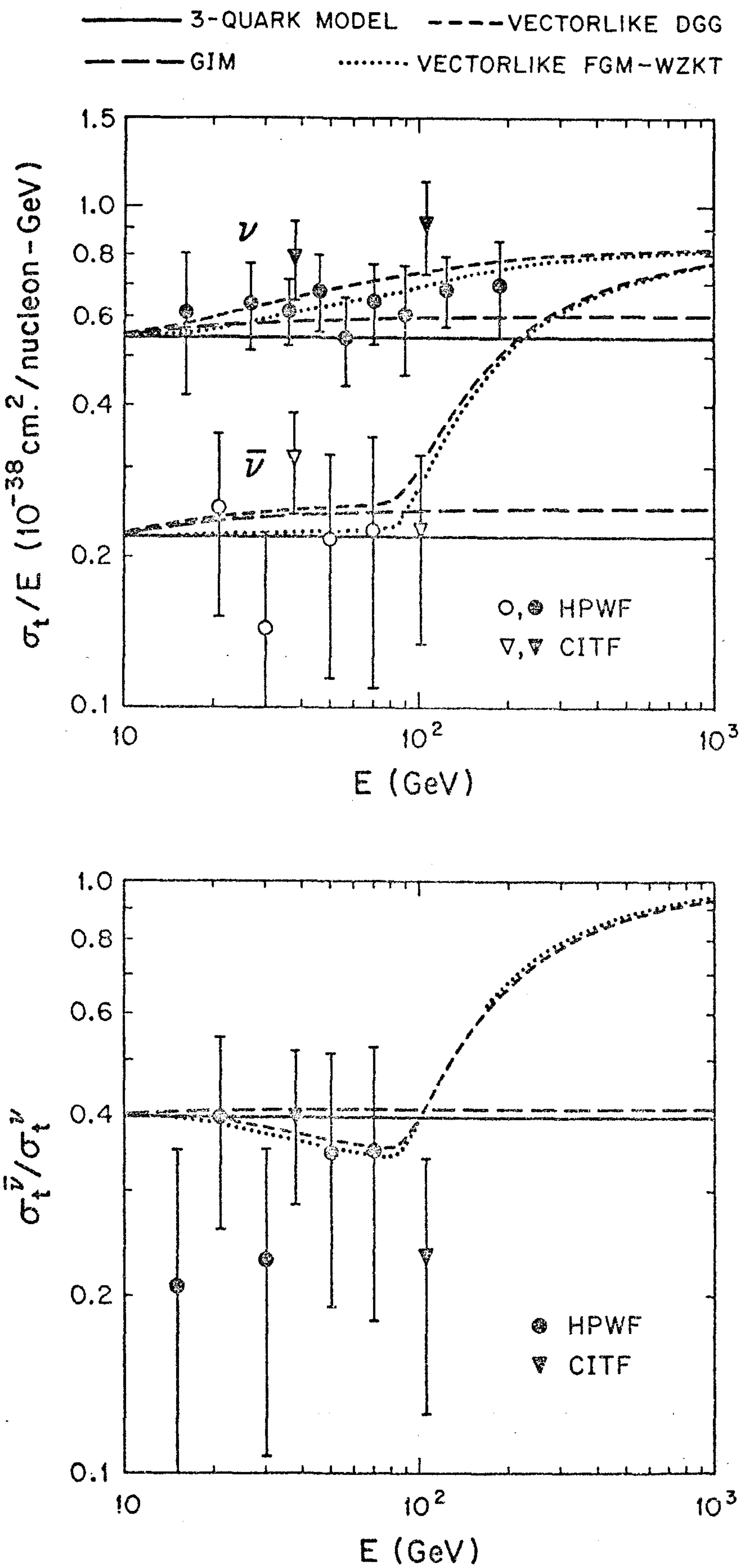

3-QUARK MODEL
VECTORLIKE DGG
GIM
VECTORLIKE FGM-WZKT
σ_t/E (10^{-38}cm.^{2}/nucleon-GeV)
ν
$\bar{\nu}$
○,● HPWF
▽,▼ CITF
E (GeV)
$\sigma_t^{\bar{\nu}}/\sigma_t^{\nu}$
● HPWF
▼ CITF
E (GeV)

Fig. 11

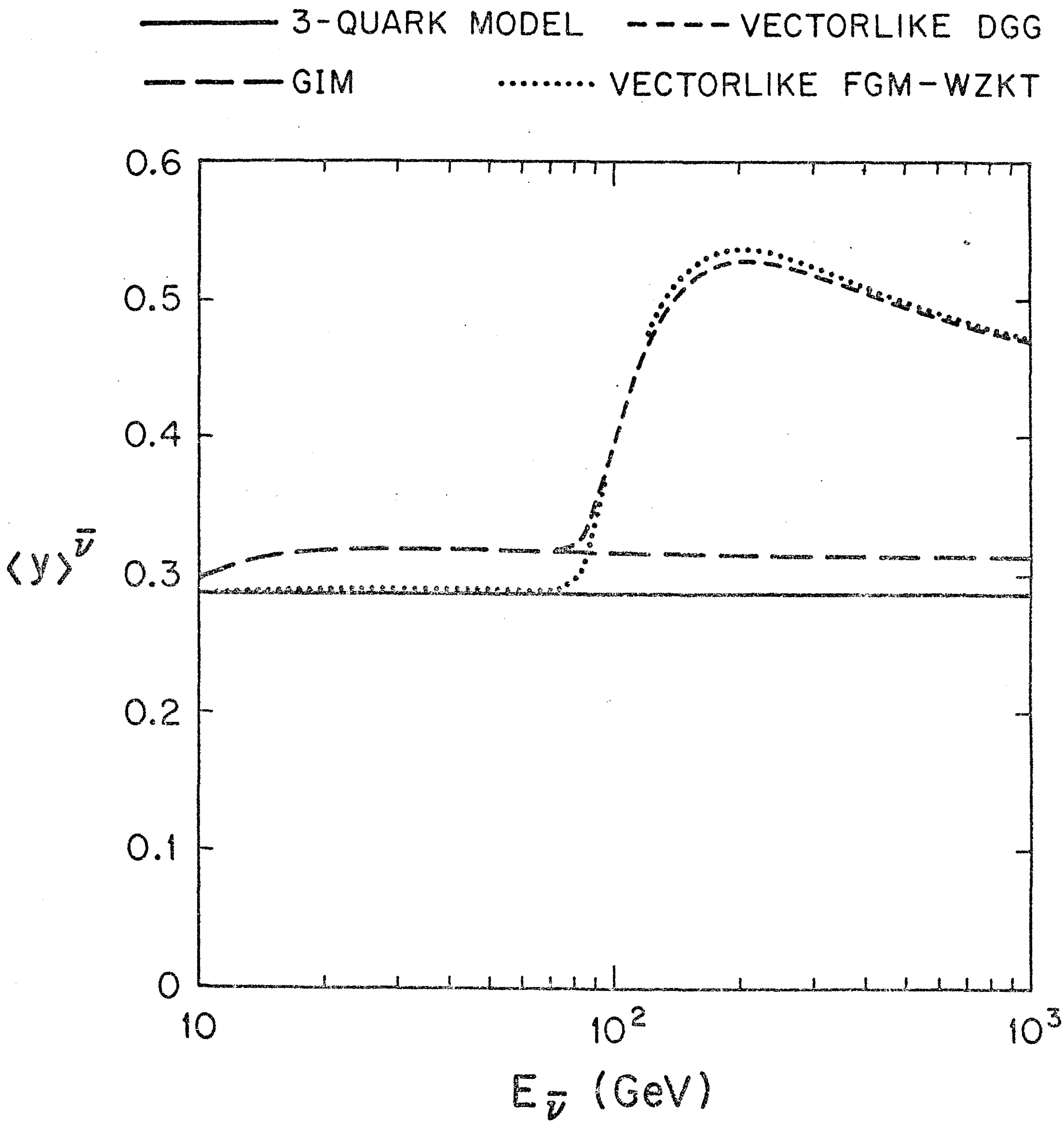
3-QUARK MODEL
VECTORLIKE DGG
GIM
VECTORLIKE FGM-WZKT
0.6
0.5
0.4
0.3
0.2
0.1
0
$\langle y \rangle^{\bar{\nu}}$
10
10^2
10^3
$E_{\bar{\nu}}$ (GeV)

Fig. 12